Journal of Materials Chemistry C

RSC Publishing

PAPER

View Article Online
View Journal | View Issue

Cite this: J. Mater. Chem. C, 2013, 1, 7593

Eliminating surface effects *via* employing nitrogen doping to significantly improve the stability and reliability of ZnO resistive memory†

Teng-Han Huang,[a] Po-Kang Yang,[a] Wen-Yuan Chang,[a] Jui-Fen Chien,[b] Chen-Fang Kang,[a] Miin-Jang Chen[b] and Jr-Hau He*[a]

Received 7th August 2013
Accepted 29th September 2013

DOI: 10.1039/c3tc31542h

www.rsc.org/MaterialsC

Metal oxides suffering from oxygen molecule chemisorption display environment-dependent metastability, leading to unstable resistive memory characteristics and performance degradation. To obtain ambient-independent characteristics, we introduced nitrogen into ZnO resistive memory devices, compensating for the native defects and suppressing oxygen chemisorption, giving rise to a significant improvement in switching behavior without undesired surface effects. Moreover, by thermal activation of the nitrogen doping *via* annealing, an increased yield ratio from 50% to 82%, a reduced current compliance from 15 mA to 5 mA, and more stable cycling endurance are obtained. Our findings give physical insight into designing resistive memory devices.

Surface effects from chemisorption/photodesorption[1,2] and native surface defects/states[3] give rise to significant surface band bending (up to 1.27 eV for single crystalline ZnO, for example),[4] and significantly influence the electronic and opto-electronic properties of metal oxides.[5]

Surface effects are a double-edged sword for device applications of metal oxides. Metal oxide-based photodetectors/gas sensors enjoy great advantages of pronounced/enhanced surface effects, while an ultrahigh sensitivity to light/chemical molecules is obtained *via* oxygen molecule chemisorption effects.[2,6–10] However, some metal oxide-based devices such as transistors[11] and resistive memory devices[12–15] suffer from surface effects. Taking metal oxide-based resistive memory as an example, the switching mechanism is the electrochemical redox process associated with the formation/rupture of defect-based conductive nanofilaments near the surface/interface between electrodes and the metal oxide.[16] Thus, the resistive switching characteristics of a metal oxide exhibit environment-dependent metastability,[14] leading to significant parameter fluctuations in the resistance distributions (cycle-to-cycle and device-to-device fluctuations), which is detrimental for device reliability and uniformity. Moreover, noticeable tail bits in the resistance distribution observed in a large memory array would remarkably reduce the resistance window and thus impede the multilevel capability of the resistive memory device.[17,18] Consequently, a promising way to eliminate surface effects to achieve stable and uniform switching characteristics is in particularly demand for memory applications.

In this study, we systematically investigate the effects of nitrogen doping in ZnO on the performance of the resistive memory device. Doping nitrogen into ZnO by employing an atomic layer deposition (ALD) technique has been proposed to significantly improve the stability and reliability of ZnO resistive memory *via* eliminating surface effects. Nitrogen doped into an ALD-grown ZnO thin film compensates for the native defects and thus reduces oxygen molecule chemisorption, which suppresses the surface effects on the resistive switching behaviors, and consequently the memory devices exhibit superior immunity against ambient conditions. Furthermore, activation of the nitrogen dopant by annealing at 400 °C causes the ALD-grown nitrogen-doped ZnO (ZnO:N) memory devices to exhibit significant performance improvements including increased yield ratio from 50% to 82%, reduced current compliance (I_{comp}) from 15 mA to 5 mA, and more stable endurance with better reset current distribution. The endurance characterization at 100 °C reveals the excellent high-temperature reliability of the ZnO:N memory device, demonstrating a feasible improvement method and gaining insight into the underlying physical mechanisms to provide guidelines for future device design and optimization against undesired switching parameter variations for next generation non-volatile memory devices.

40 nm thick ZnO:N thin films were deposited on TiN/Ti/SiO_2/Si substrates using diethylzinc (DEZn) and H_2O as reactant

[a]Institute of Photonics and Optoelectronics, Department of Electrical Engineering, National Taiwan University, Taipei 106, Taiwan, ROC. E-mail: jhhe@cc.ee.ntu.edu.tw; Tel: +886-2-33669646

[b]Department of Materials Science and Engineering, National Taiwan University, Taipei 10617, Taiwan, ROC

† Electronic supplementary information (ESI) available. See DOI: 10.1039/c3tc31542h

gases, and ammonia (NH_3) as a source for doping nitrogen into ZnO. The growth temperature was maintained at 180 °C during the ALD process. For the thermal activation of the nitrogen dopants, the ZnO:N thin film was put into a furnace for 10 min in air at 400 °C. 30 nm thick top circle electrodes of Cr with a 100 μm diameter and 50 nm thick Au capping layer were deposited on the ZnO:N thin films by electron-beam evaporation with a metal shadow mask. The *I–V* characteristics were measured using a Keithley 4200 semiconductor parameter analyzer. During the measurements in voltage sweeping mode, the bias was defined as positive when the current flowed from the top (Au/Cr) to the bottom (TiN) electrode, and the negative bias was defined by the opposite direction.

Nitrogen doping was carried out by (1) an ALD technique to provide nitrogen impurities, and (2) annealing to activate the dopants (*i.e.*, the process of obtaining the desired electronic contribution from the nitrogen impurities in the ZnO host). Fig. 1 shows the typical macroscopic *I–V* switching characteristics of the as-deposited and thermally activated ZnO:N (TA ZnO:N) devices. An electrical stress with I_{comp}, known as the forming process, is necessary to initiate the switching behavior of the Au/Cr/ZnO:N/TiN structure (see Fig. S1 in the ESI† for details). After the forming process, the devices were in the low resistance state (LRS). By sweeping the voltage on the negative side without I_{comp}, an abrupt drop in current occurs at a reset voltage (V_{reset}), indicating the switch of the resistance to the high resistance state (HRS), a nonvolatile OFF state. While sweeping back to the positive bias, the current increases suddenly at a set voltage (V_{set}), indicating the resistive switch back to the LRS, a nonvolatile ON state. One can see that the as-deposited and TA ZnO:N thin films show similar bipolar switching behaviors, in which the negative bias induces the HRS and the positive bias resets the state to the LRS. This bistable resistive switching behavior is reversible and controllable. Note that there is no resistive switching phenomenon observed in the ALD-grown intrinsic ZnO thin film due to its low resistivity, as shown in the inset of Fig. 1. The switching

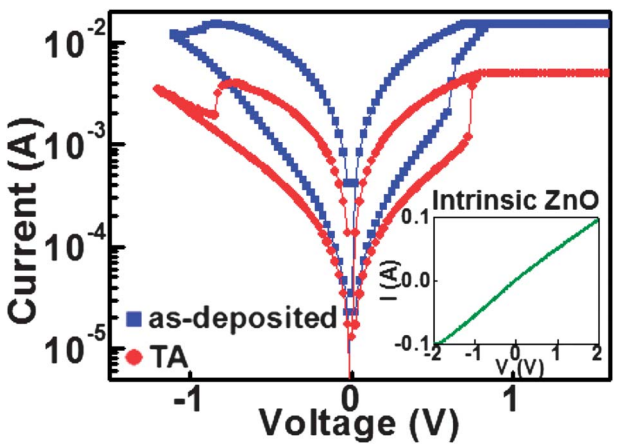

Fig. 1 Typical bipolar resistive switching characteristics of as-deposited and TA ZnO:N films grown by ALD. The inset is the *I–V* characteristics of intrinsic ZnO grown by ALD, showing no resistance switching phenomenon.

yields of ALD-grown ZnO and ZnO:N with and without thermal activation under different I_{comp} are tabulated in Table 1. The as-deposited ZnO:N without thermal activation cannot be operated with an I_{comp} less than 15 mA, so the yield of as-deposited ZnO:N with 5 mA I_{comp} is 0%, while that with 15 mA I_{comp} is 50%. After nitrogen dopant activation by annealing at 400 °C, the minimum I_{comp} of the ALD-grown ZnO:N memory devices can be reduced from 15 mA to 5 mA with 100 stable switching cycles, and thus the device experiences less damage, leading to a higher yield. Compared to the yield of TA ZnO:N with 5 mA I_{comp} (82%), the yield of TA ZnO:N with 15 mA I_{comp} is merely 57%. The percent yield is determined by the ratio of the amount of cells switching continually over 5 cycles without any set or reset failure to the amount of total cells in the measurement. The statistical analysis, including cycle-to-cycle and cell-to-cell tests for over 40 cells, provides essential evidence for evaluating the resistive switching behaviors. The improvement can be attributed to the controlled I_{comp}, which could affect the resistive switching significantly.[19] Larger nanofilaments with a higher density are formed with larger I_{comp}, resulting in a larger reset current in the reset process.[20–22] Due to the higher operating current, the memory devices could suffer from more damage during resistive switching, leading to a lower yield.[23] Thermal activation of the nitrogen doping is crucial to reduce the required operating current. As a result, TA ZnO:N devices have a much lower operating current and higher yield than the as-deposited ZnO:N devices, so the TA ZnO:N memory devices exhibit lower power consumption and suffer from less damage during resistive switching.

To gain insight into the reliability characteristics of the ALD-grown ZnO:N memory devices, cycling endurance and data retention were measured at room temperature. The resistance values of the HRS and LRS were read out at 0.1 V. Fig. 2(a) shows the endurance characteristics of the as-deposited and TA ZnO:N devices. The memory window of the as-deposited ZnO:N device shows considerable variation/degradation over 100 switching cycles, while thermal activation *via* annealing leads to more stable switching, *i.e.*, a smaller variation in the resistance values of both the HRS and LRS. In addition, we plot the cumulative probability distribution at the switching voltage, as shown in Fig. 2(b). Both of the ZnO:N devices show a similar concentration distribution of V_{set} and V_{reset}, with average values of 0.85 and −0.82 V, respectively. However, the cumulative probability distribution of the reset currents exhibits different characteristics between the as-deposited and TA ZnO:N devices, as shown in Fig. 2(c). For the as-deposited ZnO:N devices, the reset current ranges between 5.4 and 28.5 mA and exhibits a mean

Table 1 Switching yields of ALD-grown intrinsic ZnO, as-deposited ZnO:N, and TA ZnO:N devices under different current compliance values

Yield (%)	Intrinsic ZnO	As-deposited ZnO:N	TA ZnO:N
5 mA I_{comp}	0	0	82
15 mA I_{comp}	0	50	57

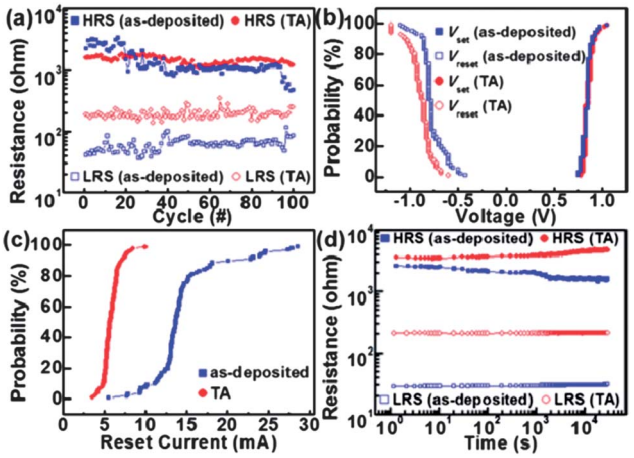

Fig. 2 (a) Endurance measurement for 100 continuous cycles, (b) distribution of V_{set} and V_{reset}, (c) distribution of reset current, and (d) retention of as-deposited and TA ZnO:N devices at room temperature.

value (μ) of 14.5 mA and a standard deviation (σ) of 4.0 mA. On the other hand, TA ZnO:N devices show a concentration distribution of reset current with $\mu = 5.8$ and $\sigma = 1.0$ mA, indicating significant advantages over the as-deposited ZnO:N devices for memory applications in terms of stable cycling endurance. The data retention test at room temperature is shown in Fig. 2(d). Both the HRS and LRS of the TA ZnO:N devices remain stable, while the HRS in as-deposited ZnO:N devices shows a slight degradation after 30 000 s of the retention test, showing that the ZnO:N device exhibits improved nonvolatile data storage capability after appropriate annealing.

To understand the conducting mechanism of the TA ZnO:N device, the temperature-dependent resistance of the initial resistance state (IRS), HRS, and LRS were measured (Fig. 3(a)). The resistance of the LRS shows an increase with temperature, indicating typical metallic behavior. On the other hand, the resistance of the IRS and HRS decrease with temperature, indicating semiconducting behavior. As shown in Fig. 3(b), the high-temperature endurance test of the TA ZnO:N device reveals its excellent reliability, even at temperatures as high as 100 °C, though resistance fluctuations of HRS and LRS are observed.

It has been observed that stability to atmosphere is an extremely significant issue for the electrical transport of ZnO due to $O_{2(ad)}^{-}$ chemisorption.[14,15] O_2 molecules adsorbed at the defects of ZnO surfaces, such as surface defects and oxygen vacancies, act as electron acceptors to form chemisorbed $O_{2(ad)}^{-}$. With increasing ambient oxygen partial pressure, more O_2 molecules chemisorbed on the ZnO surface are expected. In order to study the effect of nitrogen doping on the resistive switching characteristics of ZnO, the resistance of the HRS and LRS of sputtered ZnO and ALD-grown ZnO:N devices is compared at different oxygen partial pressures by varying atmospheric conditions, as shown in Fig. 4(a) and (b). It should be noted that three cells operated over 20 cycles were included in the statistical analysis for each set of atmospheric conditions. The concentration of chemisorbed $O_{2(ad)}^{-}$ at the ZnO surface under four measurement conditions at room temperature is in the order vacuum < N_2 < air < O_2.[14,15] As the environment is changed from vacuum to O_2 ambience, the HRS of sputtered ZnO shifts to a higher resistance value and the fluctuation of the HRS is suddenly increased, as shown in Fig. 4(a). This phenomenon can be attributed to the $O_{2(ad)}^{-}$ chemisorption causing the surface band bending effect and thus a lower conductivity of ZnO near the surface. Note that since the transport mechanism in the LRS is dominated by metallic conductive filaments, the resistance value of LRS is not influenced by the surface band bending effect. Surprisingly, by incorporating nitrogen into ZnO, the resistance fluctuations of the HRS are remarkably suppressed, and the HRS resistance value reveals little dependence on the oxygen partial pressure, as shown in Fig. 4(b). As indicated in Fig. 4(c) and (d), forming voltage, V_{set}, and V_{reset} also show little dependence on the ambient oxygen concentration, again demonstrating that the undesired surface effects on the resistive switching behaviors can be eliminated by doping nitrogen into ZnO. Briefly, by doping nitrogen into ZnO, the device characteristics become insensitive to the environment in terms of resistance fluctuations of HRS, environment-dependent resistance values of HRS,

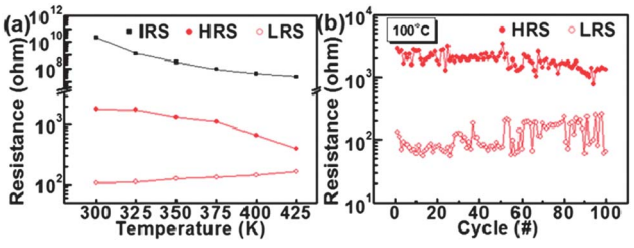

Fig. 3 (a) Temperature dependence of the resistance values of the IRS, HRS, and LRS of the TA ZnO:N devices. (b) Endurance measurements of the TA ZnO:N devices for 100 continuous cycles at 100 °C.

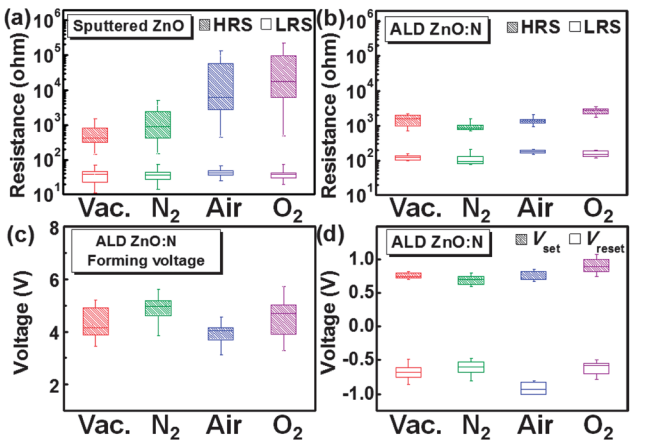

Fig. 4 Box and whisker plots for the atmosphere-dependent resistance in HRS and LRS of (a) sputtered ZnO and (b) ALD-grown ZnO:N devices. Box and whisker plots for the relationship between atmosphere and (c) forming voltage, and (d) V_{set} and V_{reset} of the ALD-grown ZnO:N devices. For the box and whisker plots, the bottom and the top of the box are the 25th and the 75th percentile, the line near the middle of the box is the 50th percentile, and the ends of the whiskers represent the 10th percentile and the 90th percentile.

forming voltage, V_{set}, and V_{reset}, which is favorable for practical RRAM applications.

The mechanism of the elimination of the surface effects on resistive switching behaviors by incorporating nitrogen into ZnO is discussed below. Fig. 5 shows the Zn 2p and N 1s XPS spectra of ALD-grown intrinsic ZnO and the N 1s XPS spectra of ZnO:N with and without thermal annealing treatment. The XPS spectra of the intrinsic ZnO thin film shown in Fig. 5(a) and (b) indicate that the ALD-grown materials are ZnO since the peak at 1021.4 eV is associated with the Zn–O bond, and there is no N–Zn bond in ZnO. The XPS spectra for the as-deposited and TA ZnO:N thin films are shown in Fig. 5(c) and (d), respectively, indicating that the doped nitrogen could bind to O, H, and Zn in the ALD process. The chemical state of N in the as-deposited ZnO:N is similar to in the 400 °C annealed ZnO:N, showing that there is no obvious escape of partial nitrogen observed with such a low-temperature annealing treatment. There is no remarkable change in the nitrogen content after thermal treatment, as shown in Fig. S2 in the ESI.† It has been reported that high-temperature annealing may induce the escape of N as N_2 bubbles.[24] The presence of H is due to the residual N–H bonds of NH_3 molecules during ALD deposition. Note that the peak at 396.4 eV is associated with the N–Zn bond, demonstrating the replacement of O by N in ZnO:N film.[25,26] That is, the introduction of nitrogen into the ALD-grown ZnO thin film compensates for the native defects such as oxygen vacancies and surface defects and thus suppresses the $O_{2(ad)}^-$ chemisorption, which plays an important role in suppressing the surface effects on the resistive switching behaviors. As mentioned earlier, the chemical states of nitrogen in the ZnO:N films should be affected by annealing at different temperatures, and further studies of the dependence of the electrical properties, including resistive switching characteristics, on the annealing temperature is needed in future to optimize the resistive memory fabrication process.

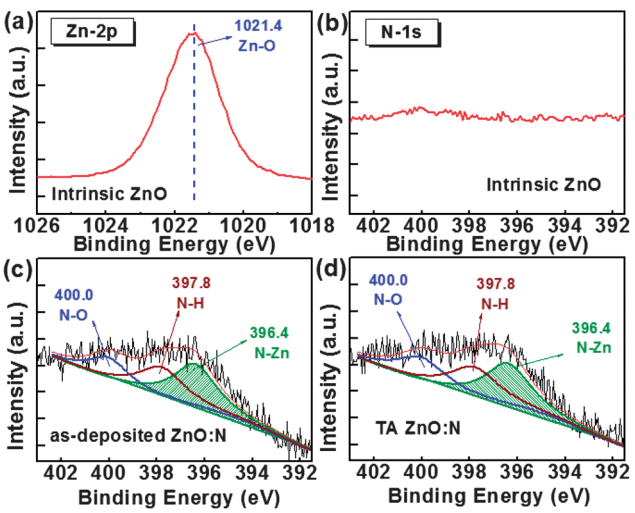

Fig. 5 (a) Zn 2p and (b) N 1s XPS spectra of ALD-grown intrinsic ZnO thin films, and the N 1s XPS spectra of (c) as-deposited and (d) TA ZnO:N thin films.

Conclusions

In summary, narrow reset current distribution, excellent switching stability, and high-temperature reliability of ZnO devices are achieved after nitrogen doping and thermally activation. Surface effects on the resistive switching behaviors are significantly eliminated due to incorporation of nitrogen compensating for the native defects of ZnO, leading to environment-independent stability, *i.e.*, stable values of HRS, forming voltage, V_{set} and V_{reset}. Process optimization of the nitrogen doping and annealing processes is under investigation to optimize the switching characteristics of metal oxide memory. The obtained insights provide strategies to design resistive memory devices without undesired switching parameter variations, as a step towards realistic application of these devices.

Notes and references

1 C. Y. Chen, C. A. Lin and J. H. He, *Nanotechnology*, 2009, **20**, 185605.
2 J. H. He, C. H. Ho and C. Y. Chen, *Nanotechnology*, 2009, **20**, 065503.
3 M. W. Allen and S. M. Durbin, *Appl. Phys. Lett.*, 2008, **92**, 122110.
4 C. Y. Chen, J. R. D. Retamal, D. H. Lien, M. W. Chen, I. W. Wu, Y. Ding, Y. L. Chueh, C. I. Wu and J. H. He, *ACS Nano*, 2012, **6**, 9366.
5 C. Y. Chen, M. W. Chen, J. J. Ke, C. A. Lin, J. R. D. Retamal and J. H. He, *Pure Appl. Chem.*, 2010, **82**, 2055.
6 Z. Fan, D. Wang, P. C. Chang, W. Y. Tseng and J. G. Lu, *Appl. Phys. Lett.*, 2004, **85**, 5923.
7 M. W. Chen, C. Y. Chen, D. H. Lien, Y. Ding and J. H. He, *Opt. Express*, 2010, **18**, 14836.
8 C. Soci, A. Zhang, B. Xiang, S. A. Dayeh, D. P. R. Aplin, J. Park, X. Y. Bao, Y. H. Lo and D. Wang, *Nano Lett.*, 2007, **7**, 1003.
9 M. W. Chen, J. R. D. Retamal, C. Y. Chen and J. H. He, *IEEE Electron Device Lett.*, 2012, **33**, 411.
10 P. C. Chen, G. Shen and C. Zhou, *IEEE Trans. Nanotechnol.*, 2008, **7**, 668.
11 J.-S. Park, J. K. Jeong, H.-J. Chung, Y.-G. Mo and H. D. Kim, *Appl. Phys. Lett.*, 2008, **92**, 072104.
12 C. H. Huang, J. S. Huang, S. M. Lin, W. Y. Chang, J. H. He and Y. L. Chueh, *ACS Nano*, 2012, **6**, 8407.
13 W. Y. Chang, C. A. Lin, J. H. He and T. B. Wu, *Appl. Phys. Lett.*, 2010, **96**, 242109.
14 J. J. Ke, Z. J. Liu, C. F. Kang, S. J. Lin and J. H. He, *Appl. Phys. Lett.*, 2011, **99**, 192106.
15 N. Xu, L. Liu, X. Sun, X. Liu, D. Han, Y. Wang, R. Han, J. Kang and B. Yu, *Appl. Phys. Lett.*, 2008, **92**, 232112.
16 R. Waser, R. Dittmann, G. Staikov and K. Szot, *Adv. Mater.*, 2009, **21**, 2632.
17 S. Yu, X. Guan and H.-S. P. Wong, *IEEE Trans. Electron Devices*, 2012, **59**, 1183.
18 Y. S. Chen, H. Y. Lee, P. S. Chen, P. Y. Gu, C. W. Chen, W. P. Lin, W. H. Liu, Y. Y. Hsu, S. S. Sheu, P. C. Chiang, W. S. Chen, F. T. Chen, C. H. Lien and M. J. Tsai, *IEDM Tech. Dig.*, 2009, 1.

19 Y. Otani, D. C. Gilmer, H. Park, O. Junko, N. Yamaguchi, T. Nakagawa, P. D. Kirsch and R. Jammy, *Tech. Dig. – Symp. VLSI Tech.*, 2011, 1.
20 B. Gao, W. Y. Chang, B. Sun, H. W. Zhang, L. F. Liu, X. Y. Liu, R. Q. Han, T. B. Wu and J. F. Kang, *Tech. Dig. – Symp. VLSI Tech.*, 2010, 144.
21 Y. S. Chen, T. Y. Wu, P. J. Tzeng, P. S. Chen, H. Y. Lee, C. H. Lin, F. T. Chen and M.-J. Tsai, *Tech. Dig. – Symp. VLSI Tech.*, 2009, 36.
22 M. Li, F. Zhuge, X. Zhu, K. Yin, J. Wang, Y. Liu, C. He, B. Chen and R. W. Li, *Nanotechnology*, 2010, **21**, 425202.
23 Y. Y. Chen, R. Degraeve, S. Clima, B. Govoreanu, L. Goux, A. Fantini, G. S. Kar, G. Pourtois, G. Groeseneken, D. J. Wouters and M. Jurczak, *IEDM Tech. Dig.*, 2012, 482.
24 P. Fons, H. Tampo, A. V. Kolobov, M. Ohkubo, S. Niki, J. Tominaga, R. Carboni, F. Boscherini and S. Friedrich, *Phys. Rev. Lett.*, 2006, **96**, 045504.
25 S. J. Lim, S.-J. Kwon and H. Kim, *Appl. Phys. Lett.*, 2007, **91**, 183517.
26 P.-T. Liu, Y.-T. Chou, L.-F. Teng, F.-H. Li and H.-P. Shieh, *Appl. Phys. Lett.*, 2011, **98**, 052102.